Safety assessment of an existing bridge deck subject to different damage scenarios through the global safety format ECOV

Engineering Structures 306 (2024) 117859

Contents lists available at ScienceDirect

Engineering Structures

journal homepage: www.elsevier.com/locate/engstruct

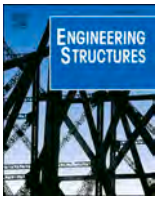

Safety assessment of an existing bridge deck subject to different damage scenarios through the global safety format ECOV

Gabriele Bertagnoli *, Mario Ferrara, Elena Miceli, Paolo Castaldo, Luca Giordano

Department of Structural, Geotechnical and Building Engineering (DISEG), Politecnico di Torino, Corso Duca deli Abruzzi 24, 10129, Turin, Italy

ARTICLE INFO

Keywords:
3D NLFEAs
Global safety format
ECOV
Existing reinforced concrete bridges
Damage thresholds

ABSTRACT

The assessment of existing reinforced concrete structures, especially bridges and viaducts, nowadays is one of the most relevant aspects for engineers. In fact, due to the old age of a large part of the infrastructure assets and the deteriorating conditions affecting the structural elements, their safety with respect to the ultimate limit states may be compromised. In this perspective, the assessment by means of global safety formats employing non-linear finite element analyses can be an extremely useful tool. In this context, the study proposes to relate the safety level to the damage through 3D global non-linear numerical analyses. Specifically, the assessment of an existing prestressed reinforced concrete bridge deck is carried out by means of the global safety format denoted as "Estimation of Coefficient of Variation" (ECOV) assuming different damage scenarios. In fact, the safety of the structure is initially assessed with respect to the ultimate limit state in its undamaged condition. Subsequently, different damage scenarios, derived from the inspections, are numerically studied. For each damage scenario, the safety of the deck is evaluated with respect to the ultimate limit state relating the safety loss to the damage level. Finally, damage thresholds for this type of structure are defined on specific static parameters.

1. Introduction

The construction of the infrastructure assets of most Western countries dates prior to 1980. This heritage is now becoming old and is subject to different degradation phenomena [1]. For these reasons, the assessment of structural safety is an increasingly central issue for both engineers and researchers [2]. The decreasing safety level of existing bridges is an important topic so that the Italian Ministry of Infrastructures and Sustainable Mobility published new provisions denoted as "Italian Guidelines for Safety Assessment of Existing Bridges" [3] in 2022 and some applications may be found in [4,5].

Structural safety assessment can be carried out with simpler or more refined methodologies. *fib* Model Code 2010 [6] suggests an approach based on Levels of Approximation (LoA) [7,8] specifying that high levels of approximation allow for the use of refined numerical models, for example, the non-linear finite element (NLFE) method. Within the probabilistic method (PM) [6], the global structural strength R is represented by an appropriate probabilistic distribution defined through non-linear finite element analyses (NLFEAs). The design value of the global structural resistance R_d can be evaluated as follows:

$$R_d = \frac{R_{rep}}{\gamma_R \bullet \gamma_{Rd}} \tag{1}$$

where R_{rep} denotes the global resistance of the structure evaluated according to a selected safety format; γ_R is the global resistance safety factor accounting for the uncertainties related to the inherent randomness of both geometry and material properties (i.e., aleatory uncertainties); γ_{Rd} denotes the global safety factor representative of the model uncertainties (i.e., epistemic uncertainties). According to a high LoA, the evaluation of the terms in Eq. (1) requires a proper NLFE modelling accomplished following several guidelines available in the literature [9–11]. The results from these complex models need to be properly processed to satisfy safety and reliability requirements. For this reason, different safety formats have been proposed in both literature [12–14] and international standards [6,15]. Their application and discussion may be found in [16–18]. A comparison between the different safety formats is also discussed in [19]. Among these, the method of estimating the coefficient of variation (ECOV) of the structural resistance [6] is implemented in the present work. Within this method [6,19,20], the design value of the global resistance R_d is evaluated as follows:

* Corresponding author.
E-mail address: gabriele.bertagnoli@polito.it (G. Bertagnoli).

https://doi.org/10.1016/j.engstruct.2024.117859
Received 24 October 2023; Received in revised form 15 February 2024; Accepted 10 March 2024
Available online 16 March 2024

$$R_d = \frac{R_m}{\gamma_R \bullet \gamma_{Rd}} \tag{2}$$

where R_m represents the structural resistance predicted by a NLFEA with the mean values of the material properties and nominal ones for the geometry in the structural model; γ_R is the global resistance safety factor which covers the uncertainties related to the material and geometrical properties; γ_{Rd} is the global safety factor of the model uncertainties. Fixed the reliability index, the value of γ_{Rd} does not depend on the value of γ_R and can assume values from 1.00 to 1.10 [6]. In the following, the upper value of 1.10 was considered for γ_{Rd}. Assuming that the probabilistic distribution for the global resistance of the structure is lognormal, the global safety factor γ_R can be computed according to Eq. (3):

$$\gamma_R = \exp\left(\alpha_R \bullet \beta \bullet V_R\right) \tag{3}$$

where V_R is the coefficient of variation (COV) of the distribution of the global structural resistance; β is the target reliability index set equal to 3.8; α_R is the first-order reliability method (FORM) sensitivity factor equal to 0.8 [21] under the hypothesis of dominant variables. The value of β might be lower for existing structures under appropriate assumptions, as suggested in [22]. It is also important to underline that the value of 1.10 for γ_{Rd} is related to β= 3.8 assuming the epistemic uncertainties non-dominant. Different values of α_R as well as higher values of γ_{Rd} could be necessary for corroded prestressed RC structures. To this scope, note that, only considering explicitly the mechanical and geometrical uncertainties in addition to the "between" (different solution strategies used to analyse one corroded prestressed RC member) and "within" (one solution strategy used to analyse different corroded prestressed RC members) epistemic uncertainties [23–28], it is possible to identify the dominant or non-dominant role of the aleatory uncertainties with respect to epistemic ones and specify the appropriate values of both the FORM sensitivity factor α_R and γ_{Rd} [29]. In the ECOV method [6], with a simplified approach and using the assumption of a lognormal distribution for the global structural resistance, the value of V_R can be estimated as follows:

$$V_R = \frac{1}{1.65} \bullet \ln\left(\frac{R_m}{R_k}\right) \tag{4}$$

where R_k is the structural resistance predicted by a NLFEA performed using the characteristic values of the material properties and nominal ones for the geometry in the definition of the structural model. In summary, it is necessary to perform two NLFEAs for the application of the ECOV safety format: one with the mean material properties and one with the characteristic material properties, having nominal properties for the geometry. Once the COV is calculated as a function of the two obtained global resistances (Eq.(4)), it is possible to calculate the global safety factor γ_R through Eq.(3) assuming the specific target reliability index β and FORM sensitivity factor α_R. Finally, the design global resistance of the structure can be calculated according to Eq.(2).

Numerous studies have been conducted in the past years regarding applications of NLFEAs on reinforced concrete (RC) structures with different aims: safety assessment [30,31], evaluation of damage effects [32,33] as well as understanding of the structural behaviour [27,34].

In this study, 3D NLFEAs are developed for safety assessment of a bridge deck under different levels of damage caused by concrete degradation and reinforcing steel corrosion. In fact, it is proposed to calculate the safety level depending on the damage through 3D global non-linear numerical analyses, to assess the effects of the damage scenario, actually found during the visual inspections of the structure, on the structural safety varying its magnitude/extent. Specifically, the assessment of an existing prestressed RC girder deck of a highway bridge is carried out by means of the global safety format "ECOV" [6] assuming nine different damage scenarios: the first one represents the real situation observed on the structure, seven scenarios are theoretically derived from the real case varying the extent and magnitude to cover the uncertainty in the identification of the observed damage during the visual inspections. Other damages in different positions are not herein hypothesised since were not observed during the inspections. The last one represents the ultimate limit damage for the deck safety with respect to the ultimate limit state (ULS). In detail, the safety of the bridge deck is assessed with respect to the ULS in its undamaged condition developing 3D NLFEAs with mean and characteristic material strengths, respectively. Subsequently, the safety of the deck is numerically evaluated with respect to the ULS for the other nine different damage scenarios to assess the sensitivity of the structure to the extension and intensity of the structural degradation. In addition, the safety loss is evaluated in relation to the damage level. Finally, damage thresholds on some static parameters are determined for the structure under consideration.

2. Structural system: deck description

The viaduct belongs to an Italian stakeholder and was built in the 1960s. The viaduct deck is made of several simply supported prestressed RC girders having a length of 45 m with net longitudinal spans of 42 m. Each girder is 19.10 m wide and counts six longitudinal double-tee beams. The slab is 20 cm thick and four transverse beams are present. The beams and slab are prefabricated elements, jointed in-situ by a concrete cast.

The longitudinal beams interaxis is 3.40 m, as shown in Fig. 1. All the longitudinal beams have the same cross-section with a depth of 2.60 m and a 25 cm thick web. The transverse beams are at the ends and at the thirds of each span. They have a rectangular cross-section with a depth of 2.30 m and a thickness variable from 25 cm (end ones) to 20 cm (span ones), as illustrated in Fig. 2.

2.1. Reinforcement arrangement

Ordinary together with pre and post tensioning reinforcements are present in the deck. In the longitudinal beams, there are 94 half-inch diameter strands and one post-tensioned cable with 32 wires of 7 mm diameter. Transverse post-tension reinforcements are present in the transverse beams and in the slab above them. Two cables having 24 wires of 7 mm diameter and 22 wires of 7 mm diameter, respectively, lie in the transverse beams. One transverse cable is in the slab having 32 wires of 7 mm diameter. All the details together with graphical layouts regarding the reinforcement arrangement may be found in "Annex A".

2.2. Material characterisation

The mechanical properties of the materials used in the original design of the deck are listed in Table 1. At the original time of the design of the deck and according to the standards in force at the time, the values of the minimum material strengths had to be guaranteed (Table 1).

Few years ago, concrete and reinforcement specimens were sampled in-situ from the bridge deck for safety assessment. The average and COV values of the concrete compressive strength were measured on 15 cylindrical cores of 10 cm diameter: 12 taken from the longitudinal beams and 3 from the slab. Note that since both beams and slab are prefabricated with the control on the concrete casting during the prefabrication procedure, the COVs in Tables 2–6 are lower than 10%. All other fundamental properties of concrete were derived from the cylindrical strength following the formulations proposed by *fib* Model Code 2010 [6] and EN 1992–1-1 [35] including the specific correlations. In addition, four specimens of ordinary steel bars were taken from ϕ8 and ϕ10 bars as well as five prestressing steel specimens were taken from the strands. As for the rheological characteristics of concrete (i.e., creep and shrinkage) and steel relaxation factor, the corresponding mechanical parameters were taken from literature [35] including the specific correlations.

In order to adopt the ECOV safety format, the characteristic strengths

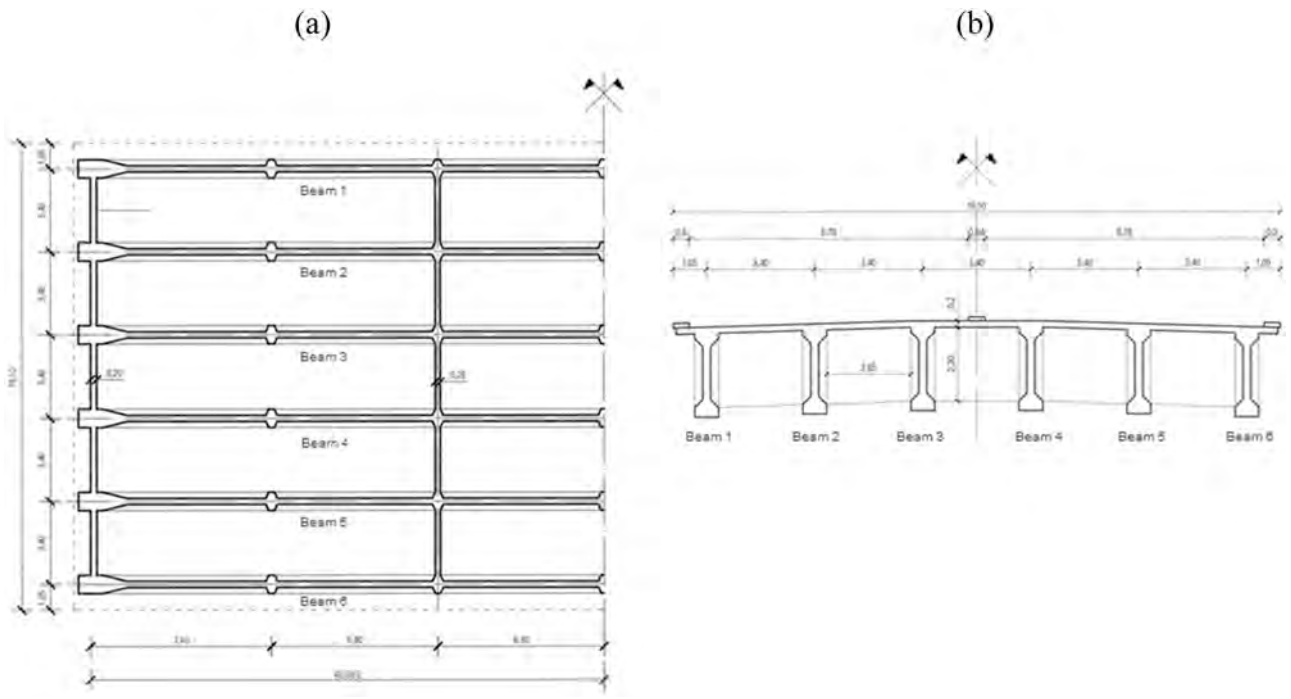

Fig. 1. Geometry of the deck: (a) planimetry, (b) cross-section. Measurements are in meters.

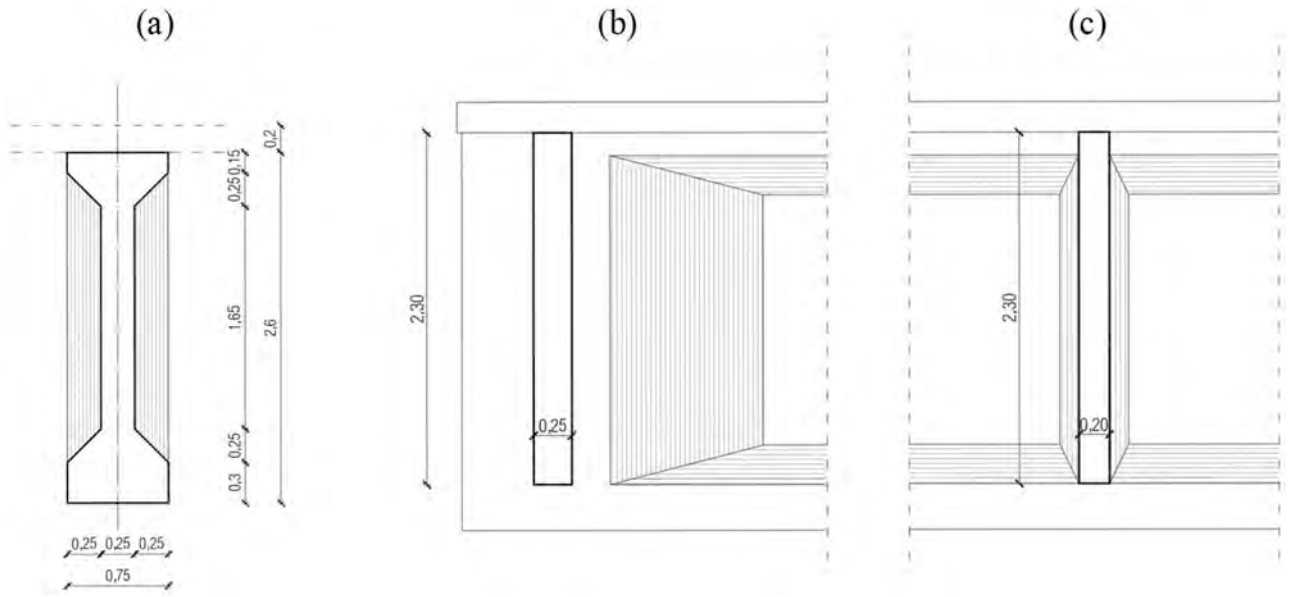

Fig. 2. Geometrical details: (a) longitudinal beam cross-section, (b) transverse beams at the ends of the spans, (c) span transverse beams. Measurements are in meters.

Table 1
Mechanical properties of materials used in the original design of the deck.

Description	Value
Minimum compressive strength of concrete [MPa]	46
Minimum tensile strength of ordinary reinforcing steel [MPa]	440
Minimum tensile strength of pre-tension reinforcing steel [MPa]	1750
Minimum tensile strength of post-tension reinforcing steel [MPa]	1650

Table 2
Mechanical properties for the concrete of longitudinal beams.

Description	Symbol	Mean value	COV	Characteristic value
Cylindrical compressive strength [MPa]	f_{cc}	57	9.0%	48
Tensile strength [MPa]	f_{ct}	4.0	*	3.5
Elastic modulus [MPa]	E_c	38,340	*	36,218

* Value of COV not available. The other mechanical parameters were calculated with formulations according to [6,35].

Table 3
Mechanical properties for the concrete of transverse beams and slab.

Description	Symbol	Mean value	COV	Characteristic value
Cylindrical compressive strength [MPa]	f_{cc}	49	4.0%	44
Tensile strength [MPa]	f_{ct}	3.5	*	3.3
Elastic modulus [MPa]	E_c	36,400	*	35,320

* Value of COV not available. The other mechanical parameters were calculated with formulations according to [6,35].

Table 4
Mechanical properties for the ordinary reinforcing steel.

Description	Symbol	Mean values	COV	Characteristic value
Yield strength [MPa]	f_{ys}	425	5.0%	383
Ultimate strength [MPa]	f_{us}	575	3.0%	543
Ultimate strain [-]	ε_{us}	0.117	12.0%	0.098
Elastic modulus [MPa]	E_s	200,000	*	200,000

* Value of COV not available. The other mechanical parameters were calculated with formulations according to [6,35].

Table 5
Mechanical properties for the pre-tension reinforcing steel.

Description	Symbol	Mean value	COV	Characteristic value
Yield strength [MPa]	f_{yp}	1636	5.0%	1466
Ultimate strength [MPa]	f_{up}	1818	5.0%	1629
Ultimate strain [-]	ε_{up}	0.05	*	0.05
Elastic modulus [MPa]	E_{sp}	195,000	*	195,000

* Value of COV not available. The other mechanical parameters were calculated with formulations according to [6,35].

of the materials were obtained following the procedure proposed in [36] and [37] (Eq.(5)), as listed in Tables 2–6:

$$X_K = \exp\left(m_y - k_n \bullet s_y\right) \tag{5}$$

where X_K is the characteristic strength; m_y and s_y are, respectively, the mean value and standard deviation of the log-normal variable; k_n is a parameter depending on the number of specimens [36,37].

The comparison of the strength values used in the original design of the deck (Table 1) with the results of the laboratory tests on in-situ specimens (Tables 2–6) shows that both mean and characteristic ultimate strength values obtained from in-situ tests are higher than the minimal values assumed in the original design of the deck for concrete and ordinary reinforcement steel.

3. Definition of 3D NLFE model

The deck is modelled through DIANA FEA software [38,39]. 3D solid (brick) elements with 20 nodes (Fig. 3(a)) and with 15 nodes (Fig. 3(b)) are used for the concrete bodies. Ordinary and pre/post-tension reinforcements are introduced with bar embedded elements (Fig. 3(c)).

Table 6
Mechanical properties for the post-tension wire steel.

Description	Symbol	Mean value	COV	Characteristic value
Yield strength [MPa]	f_{yp}	1530	3.0%	1412
Ultimate strength [MPa]	f_{up}	1700	3.0%	1569
Ultimate strain [-]	ε_{up}	0.05	*	0.05
Elastic modulus [MPa]	E_{sp}	195,000	*	195,000

* Value of COV not available. The other mechanical parameters were calculated with formulations according to [6,35].

The 3D solid elements are not larger than 0.5 m and not smaller than 0.2 m, thus achieving an aspect-ratio (AR) between 1 and 2 in the transverse direction and between 1 and 3 in the longitudinal direction. Reinforcement embedded bar elements have a maximum distance between the integration points equal to 0.25 m. The dimensions of the solid elements are chosen so that results are not affected by mesh dependency problems, through a preliminary iterative analysis modifying the mesh size up to convergence of the numerical results. Fig. 4 shows the complete FE model. In total, there are 344,353 nodes with 22,995 3D solid concrete elements and 9,411 bar elements.

A Smeared Cracking model is used for concrete [40,41]. The constitutive law is based on the Total Strain Crack model associated to the Modified Compression Field Theory [42] and extended to three-dimensional problems according to [43]. A linear-ultimate crack strain model is used for concrete subjected to tensile stresses, with a linear tension softening branch after reaching peak tensile strength (Fig. 5(a)) [28,44], in absence of specific experimental tests on the fracture energy.

The stress-strain relationship for concrete in compression is based on EN 1992–1-1 [35] (Fig. 5(b)). A reduction of compressive strength due to lateral cracking, based on the model proposed in [46], is implemented and the confinement model, based on the model proposed in [47], is adopted. A constant shear retention factor $\beta = 0.2$ is used to model the shear stiffness after cracking.

Three different elastic-plastic stress-strain relationships with linear isotropic hardening law after yielding, based on Von-Mises plasticity [48,49] are used for both the ordinary and prestressing reinforcements (Fig. 6). The linear hardening model was chosen in accordance with the current standards [6,35]. Ordinary reinforcing steel has an extremely ductile behaviour, with a ratio between ultimate strain (ε_{us}) and yield strain (ε_{ys}) exceeding 50 (Fig. 6(a)). Pre-stressing steel has a ductile behaviour, with a ratio between ultimate strain (ε_{up}) and yield strain (ε_{yp}) of 6 (Fig. 6(b)). Post-tensioning steel has a ductile behaviour, with a ratio between ultimate strain (ε_{up}) and yield strain (ε_{yp}) of 6 (Fig. 6(c)). The slope of the hardening branch of the characteristic resistances is different from the one of average resistances. This modelling difference derives from the different values of the COV of the yield strength and ultimate strength.

4. Preparatory simulations for the global safety assessment

A 3D NLFE model is defined to numerically simulate the global response of the bridge deck over time from its construction stages.

4.1. Visco-elastic analysis of the construction stages until to the current age

The deck was built in different construction stages. A viscous-elastic phased analysis is performed from construction time to the current age of the deck (i.e., 49 years). Shrinkage, creep and pre/post-tensioning steel relaxation are considered. The numerical code used for the analysis can take into account the effects of both shrinkage and creep, whereas the steel relaxation losses have been calculated and provided as input data. The construction phases taken into account are: prefabrication, pre-tensioning, in situ casting of slab and transverse beams and post tensioning.

Some results of the viscous-elastic analysis are shown in Fig. 7 and Fig. 8 considering both mean and characteristic values of the material properties. Specifically, the stresses in the concrete at the top and bottom fiber of the six longitudinal beams of the deck in the midspan cross-section are presented in Fig. 7, whereas the stresses in the post-tensioned cable and pre-stressed strands are shown in Fig. 8.

The construction phases of the deck last from 0 to 130 days, in the following 17,885 days (i.e., 49 years) only the rheological effects take place. The most important effects of the construction phases on the concrete stresses in the beams occur at 60 days, when the slab's self-

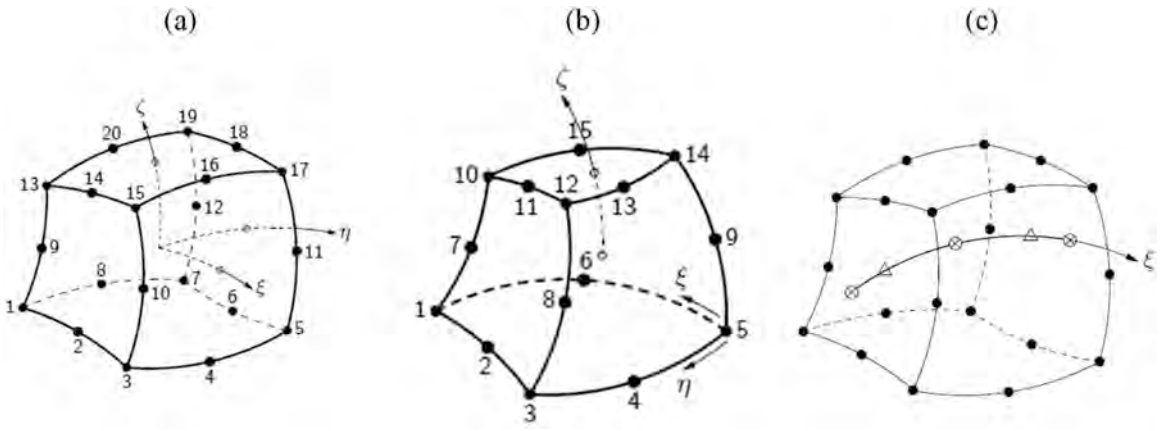

Fig. 3. Solid 3D element [39]: (a) 20 nodes brick element, (b) 15 nodes wedge element, (c) embedded bar element.

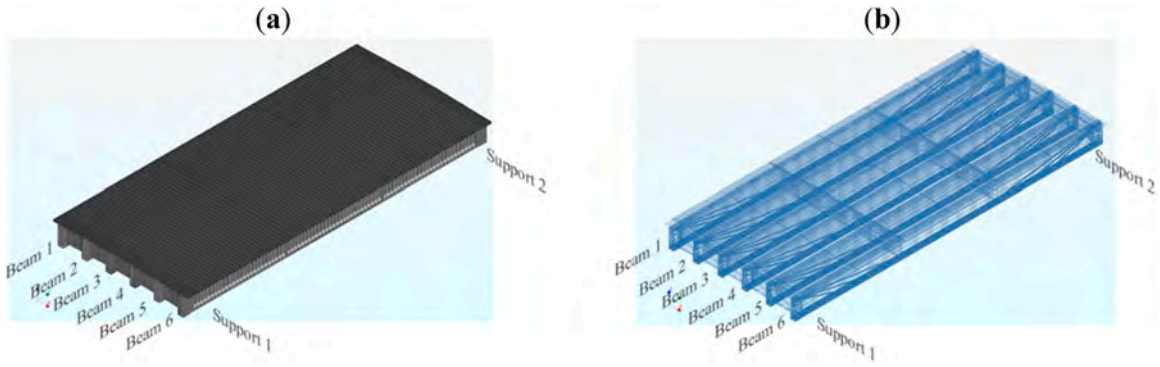

Fig. 4. 3D FE model with annotation of the beams: (a) concrete elements, (b) reinforcement elements.

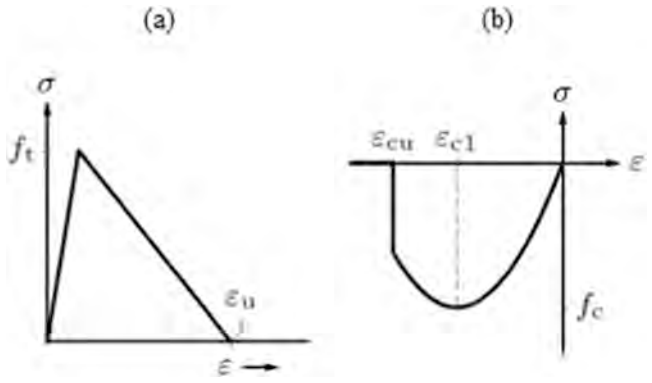

Fig. 5. Stress-Strain relationships for concrete [45]: (a) tension, (b) compression.

weight is introduced, and at 90 days with tensioning of the post-tensioned cable. These timelines were taken from the original calculation report. The stresses in the cross-section are reduced in time due to the creep, shrinkage and relaxation. In detail, there are 20.7% losses in concrete at the top fiber considering the mean material properties, whereas these losses are 4.9% higher in case of the characteristic material properties. At the bottom fiber, there are 14.7% losses when the mean material properties are implemented, whereas these losses are 2.5% higher in case of the characteristic material properties. Moreover, 6.8% losses both in the post-tensioned tendon and pre-stressed strands can be appreciated assuming the mean material properties, whereas these losses are 0.7% higher referring to the characteristic material properties.

These values are calculated between 130 days (end of construction phases) and 17,885 days (present age). Beam 1 and Beam 6 are the two edge beams of the deck (Fig. 4) and no engineering differences are present between the six longitudinal beams of the deck as a result of the viscous-elastic analysis. The viscous-elastic analysis also shows low engineering differences using the mean or characteristic properties of materials until the 49th year of the structure lifetime.

When the current age of the deck is reached, the configuration of the traffic loads (i.e., Load Model 1 - LM1) according to the current standards [50,51] is considered. In detail, all the loads are combined according to the ULS combination presented in Eq.(6):

$$F_d = \gamma_G \bullet G + \gamma_P \bullet P + \gamma_{QT} \bullet Q_T + \psi_W \bullet \gamma_{QW} \bullet Q_W \tag{6}$$

where F_d is the design action; γ_G is the partial safety factor for structural and non-structural permanent loads (equal to 1.35); G represents the structural and non-structural permanent loads; γ_P is the partial safety factor for pre/post-tension (equal to 1); P is the prestressing action; γ_{QT} is the partial safety factor for traffic loads (equal to 1.35); Q_T are the traffic loads; γ_{QW} is the partial safety factor for wind loads (equal to 1.50); Q_W is the wind action and ψ_W is the contemporaneity coefficient for wind actions (equal to 0.6 according to Italian standard [50]). Wind loads are for this deck by far less important than traffic ones, temperature effects are considered neglectable as the deck is simply supported.

Table 7 describes the different typologies of the loads considered in the phased analysis and Table 8 reports the construction time-stepping followed.

4.2. Validation of the NLFE model

The validation of the 3D FE model is based on the results of a load

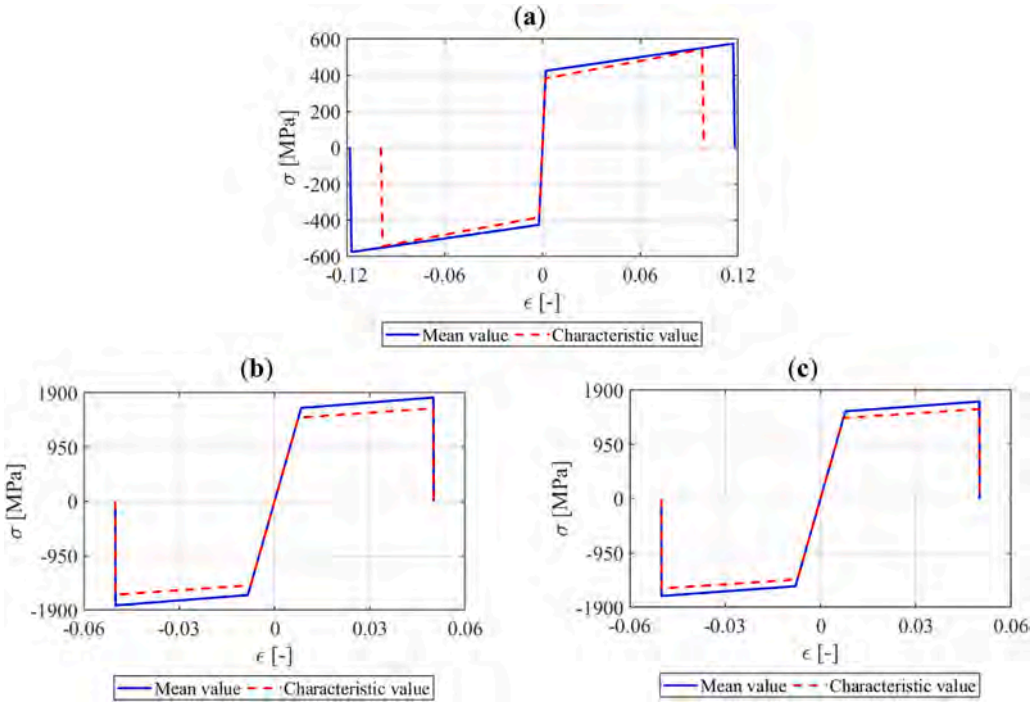

Fig. 6. Stress-Strain relationships for reinforcement: (a) ordinary reinforcement, (b) pre-tension reinforcement, (c) post-tension reinforcement.

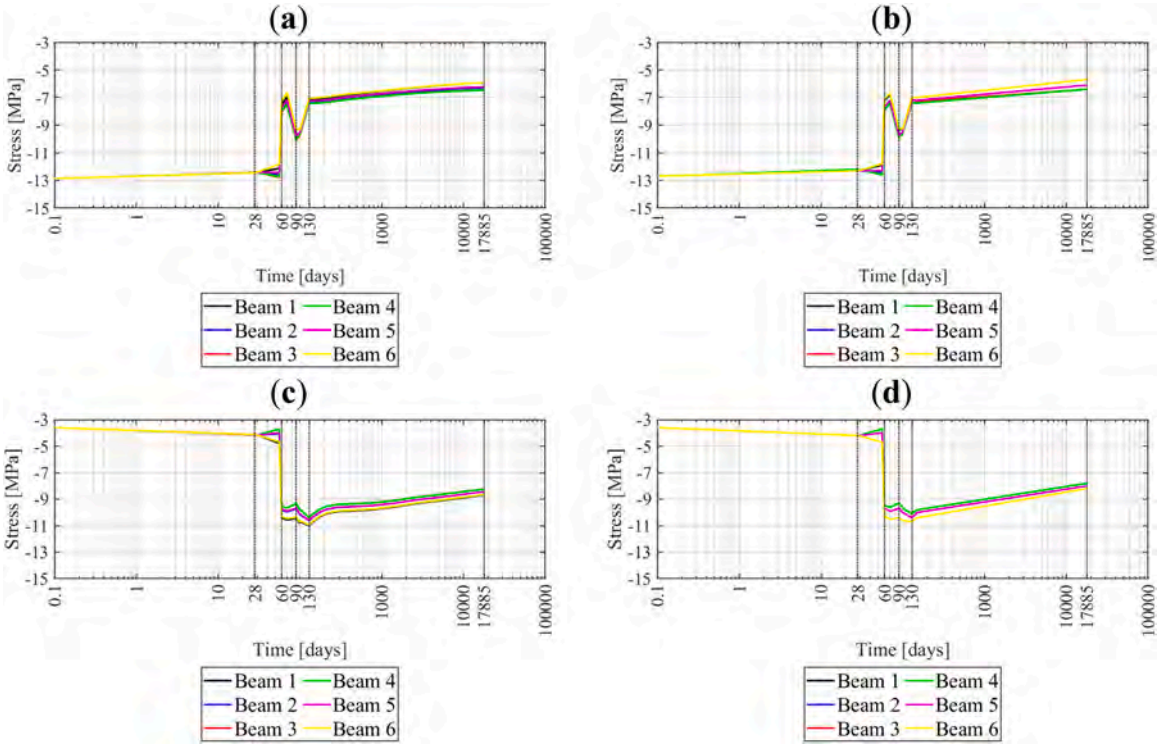

Fig. 7. Results of viscous-elastic analysis for concrete: (a) stresses at the bottom fiber of the beams with mean materials properties, (b) stresses at the bottom fiber of the beams with characteristic materials properties, (c) stresses at the top fiber of the beams with mean materials properties, (d) stresses at the top fiber of the beams with characteristic materials properties.

test performed on the deck in terms of rotations measured in the supports regions of longitudinal beams [52]. After the viscous-elastic phased analysis from 0 to 49 years, the loads of the load test, the arrangement of which is shown in Fig. 9, are introduced in the model and the rotations near the supports of the NLFE model are computed and compared with the ones measured by an in-situ monitoring system of sensors. Note that the measured rotations of the deck under investigation are assumed as reference values since the experimental monitoring campaign on the viaduct revealed that the rotations measured on damaged decks are quite identical to the rotations measured on identical

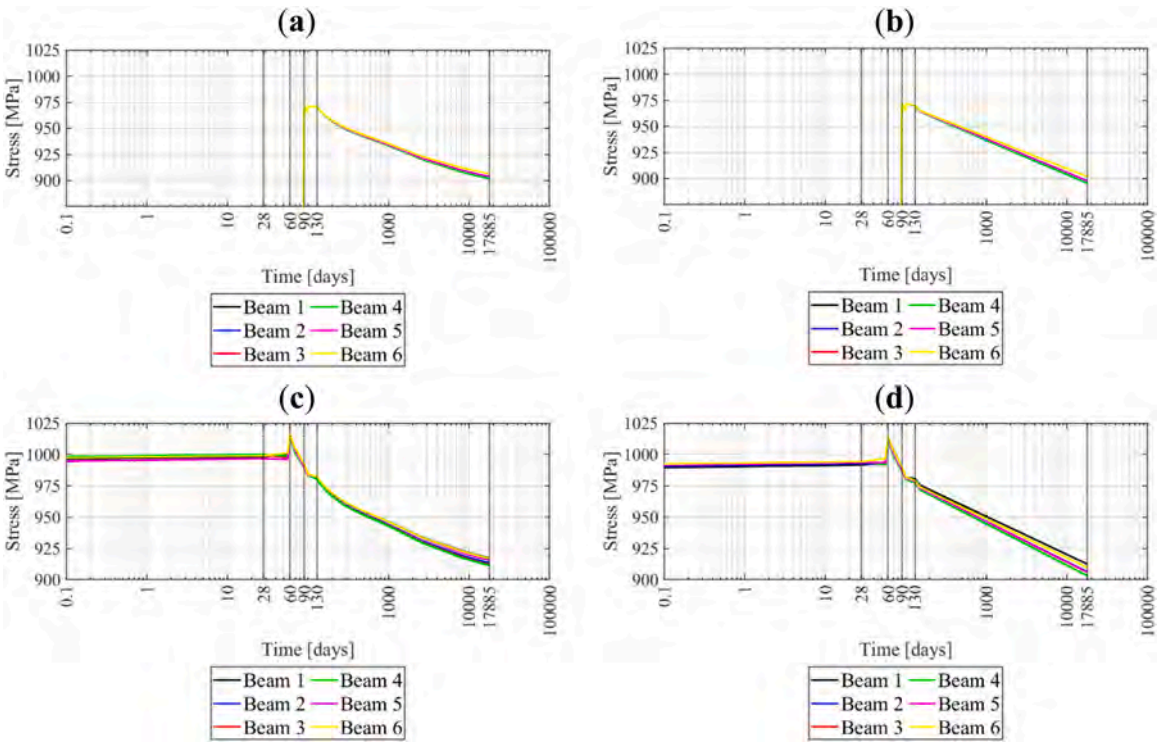

Fig. 8. Results of viscous-elastic analysis: (a) stresses in post-tensioned cables with mean materials properties, (b) stresses in post-tensioned cables with characteristic materials properties, (c) stresses in pre-stressed strands with mean materials properties, (d) stresses in pre-stressed strands with characteristic materials properties.

Table 7
Loads from the time of construction to the current age of the deck.

Description	Symbol	Value
Self-weight of longitudinal beams [kN/m^3]	$G_{1,LB}$	25
Self-weight of transverse beams [kN/m^3]	$G_{1,TB}$	25
Self-weight of slab [kN/m^3]	$G_{1,S}$	25
Pavement weight [kN/m^2]	$G_{2,P}$	3
Barriers weight [kN/m]	$G_{2,B}$	2
Tensioning stress of the pre-tensioned strands of the longitudinal beams [MPa]	P_S	1240
Tensioning stress of the post-tensioned tendon of the longitudinal beams [MPa]	P_{CLB}	1190
Tensioning stress of the post-tensioned tendon of the transverse beams (and slab) [MPa]	P_{CTB}	1190
Traffic load [kN or kN/m^2]	Q	by standard [51]

Table 8
Loads from the time of construction to the current age of the deck.

Phase	Time [days]	Active elements	Active loads
1	0	Longitudinal beams	$G_{1,LB} + P_S$
2	28	Longitudinal + Transverse beams	$G_{1,LB} + P_S + G_{1,TB}$
3	56	Longitudinal + Transverse beams	$G_{1,LB} + P_S + G_{1,TB} + P_{CTB}$
	60	Longitudinal + Transverse beams	$G_{1,LB} + P_S + G_{1,TB} + P_{CTB} + G_{1,S}$
4	70	Longitudinal + Transverse beams and slab	$G_{1,LB} + P_S + G_{1,TB} + P_{CTB} + G_{1,S}$
5	90	Longitudinal + Transverse beams and slab	$G_{1,LB} + P_S + G_{1,TB} + P_{CTB} + G_{1,S} + P_{CLB}$
6	100	Longitudinal + Transverse beams and slab	$G_{1,LB} + P_S + G_{1,TB} + P_{CTB} + G_{1,S} + P_{CLB} + P_{CS}$
	130		$G_{1,LB} + P_S + G_{1,TB} + P_{CTB} + G_{1,S} + P_{CLB} + P_{CS} + G_{2,P} + G_{2,B}$
:	:	:	:
7	>17,885	Longitudinal + Transverse beams and slab	$G_{1,LB} + P_S + G_{1,TB} + P_{CTB} + G_{1,S} + P_{CLB} + P_{CS} + G_{2,P} + G_{2,B} + Q$

undamaged decks of the same viaduct. The results of the comparison are shown in Table 9 for the beams, instrumented with inclinometers, of the real structure (i.e., Beam 2, Beam 3, Beam 4 and Beam 5) (Fig. 4). The differences between measured and numerical rotations are low and this validates the numerical model.

4.3. Damage scenarios

The side beam of the deck has been suffering from reinforcement corrosion as can be appreciated in Fig. 10: 19 out of 94 prestressing strands, 8 out of 32 wires of the prestressing tendon and 4 longitudinal ordinary reinforcement bars were broken and, therefore, ineffective in the midspan of the beam. The information about the damage is taken from the reports written by the highway authorities through visual and handy inspections. During the inspections, the entire deck is examined, but only the damage in the midspan of the structure was actually observed and described in the technical report. Other damages in different positions are not herein hypothesised since were not observed during the inspections as also confirmed by the symmetric values on Beam 2 in Table 9.

The evaluation of the safety level of the existing bridge with respect to the undamaged condition is the first step of this research. Afterwards, the real and other different damage scenarios are simulated on the deck, mainly concerning corrosion of the reinforcement varying its extension and magnitude.

Preliminary numerical tests, simulating both concrete cover spalling and consequential losing of bond between the concrete and reinforcements in the damaged areas, revealed the negligible effect of the concrete cover on the global resistance of the structure due to its nil tensile contribution in the bottom bulb of the beam at the ULS.

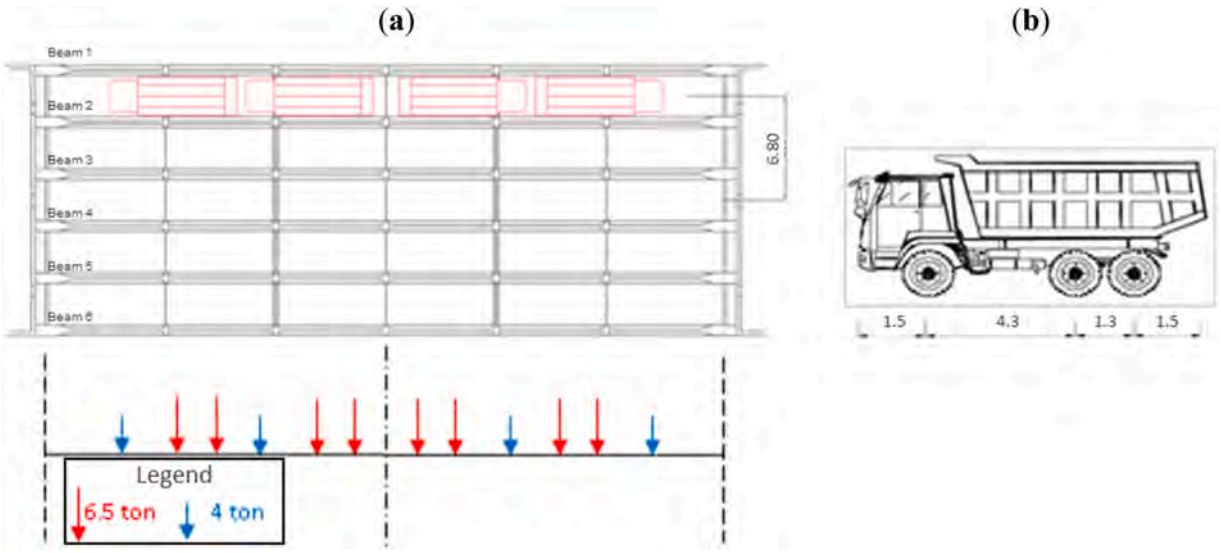

Fig. 9. Details of the arrangement of loads during the load test: (a) position, (b) lorries silhouette. Measurements in metres.

Table 9
Measured vs. NLFE model rotations.

Beam	Measured rotation [mrad]	FE model rotation [mrad]	Difference [%]
Beam 2 support 1	0.53	0.56	6.73
Beam 3 support 1	0.36	0.36	0.29
Beam 4 support 1	0.15	0.18	5.35
Beam 5 support 1	≃ 0	0.01	-
Beam 2 support 2	0.52	0.56	8.49
Beam 3 support 2	0.32	0.36	7.33
Beam 4 support 2	0.20	0.18	3.45
Beam 5 support 2	≃ 0	0.01	-

Fig. 10. Real damage on the side beam.

The stress-strain relationship of the corroded bars can vary from the one of uncorroded steel, especially, with regard to the ductility of steel. Several studies in the literature show that ductility is unchanged for low corrosion levels [53,54] and in absence of pitting corrosion [55,56]. Ductility of steel is the most variable parameter in case of very severe uniform corrosion or in presence of pitting, as yield stress and ultimate strength change slightly or negligibly. In this case study, the information available to the authors about the damage is taken from standard reports written by the highway authorities through visual and handy inspections without any quantitative technical or experimental measurements of engineering parameters. Therefore, since any evaluation of ductility or bond variation according to the formulation proposed in the literature is not possible, on safety side, the prestressing and/or ordinary reinforcements marked as "not effective" in the qualitative above-mentioned reports are removed from the numerical model to simulate the damage scenario (i.e., Damage 1). Similarly, the different other damage scenarios (i.e., Damages 2–9) are numerically derived. Table 10 shows the damage scenarios assumed and analysed. The first one (i.e., Damage 1) is the real damage found on the structure. The other seven cases (i.e., Damage 2 - Damage 8) are hypothesized. The hypothesized damages were defined by varying the extent and intensity of the real one to take into account some uncertainties highlighted during the qualitative inspections and to assess the effects of different intensities and extensions of the observed damage. The scenario "Damage

Table 10
Damage scenarios description.

Damage	Loss of pre-tension strands	Loss of wires in the post-tension cable	Loss of ordinary reinforcement bars	Damage extension
Damage 1	19/94 (−20%)	8/32 (−25%)	4/6 (−67%)	2 m
Damage 2	19/94 (−20%)	32/32 (−100%)	4/6 (−67%)	2 m
Damage 3	-	32/32 (−100%)	-	2 m
Damage 4	-	32/32 (−100%)	-	4 m
Damage 5	19/94 (−20%)	-	-	2 m
Damage 6	38/94 (−40%)	-	-	2 m
Damage 7	19/94 (−20%)	-	-	4 m
Damage 8	38/94 (−40%)	-	-	4 m
Damage 9	55/94 (−59%)	32/32 (−100%)	-	2 m

9″ represents the ultimate limit condition, when the structure collapses exactly for the load level suggested by Italian standard for the ULS.

In any scenario, the damage was considered only in the central area of the beam for an extension ranging from 2 or 4 m by removing pre-tension strands and/or post-tension wires. Outside this area, the reinforcement remains fully effective. The extent of the simulated damage (i.e., 2 or 4 m) implicitly considers an approximate length required for the re-anchorage and full effectiveness of the wires and/or strands as the damages are typically localised with a smaller extension, according to the reports written by the highway authorities. This assumption is realistic also with respect to the grouting of the post-tension wires since they are considered ineffective in the area where the cable is corroded. Outside this area, in the absence of more accurate inspections, it can be reasonable to assume no effect on the grouting.

The damage is modelled as a punctual event at the 49th year during the structure lifetime. As for the cross-section at midspan of Beam 1, Table 11 shows the displacements at the 49th year in presence of the damage under the permanent loads only. The effects in terms of increased deformability with respect to the undamaged scenario are very small. The most pronounced effect occurs for Damage 9, which is the limit condition.

4.4. Description of the ECOV methodology for safety assessment

Within the ULS load combination discussed in Subsection 4.1 (Eq. (6)) and for each damage scenario (i.e., Damage 1–9), the different loads are monotonically increased until the structure collapse in non-linear field according to the ECOV safety format [6]. Fig. 11 shows the time-history of the load multiplier during the viscous-elastic analysis from time 0 to 49 years and during the non-linear analysis performed at 49 years of age to bring the deck to collapse. In detail, after 17,885 days, the loads are increased up to achieve the design ULS load combination (i.e., Eq.(6)) and this step was performed in one virtual day. Then, the loads are hypothesized to have a 10% increase per virtual day. Fig. 12 shows the arrangement of traffic loads according to the design standards. In this way, structural safety [6] can be assessed as follows. The overall strength of the structure is determined as a function of the ultimate load multiplier μ, so, Eq.(2) can be written as follows:

$$\mu_d = \frac{\mu_m}{\gamma_R \bullet \gamma_{Rd}} \tag{7}$$

where μ_d represents the design load multiplier; μ_m represents the ultimate load multiplier predicted by a NLFEA with the mean values of the material properties and nominal ones for geometry in the structural model; γ_R can be computed through Eq.(3) where V_R can be estimated as:

$$V_R = \frac{1}{1.65} \bullet \ln\left(\frac{\mu_m}{\mu_k}\right) \tag{8}$$

where μ_k represents the ultimate load multiplier predicted by a NLFEA

Table 11
Displacement of the structure when damage is introduced: cross-section at midspan of Beam 1.

Case	Displacement [mm]
Undamaged	1.61
Damage 1	1.64
Damage 2	1.90
Damage 3	1.62
Damage 4	2.28
Damage 5	1.65
Damage 6	2.06
Damage 7	2.18
Damage 8	3.41
Damage 9 (ultimate condition)	7.51

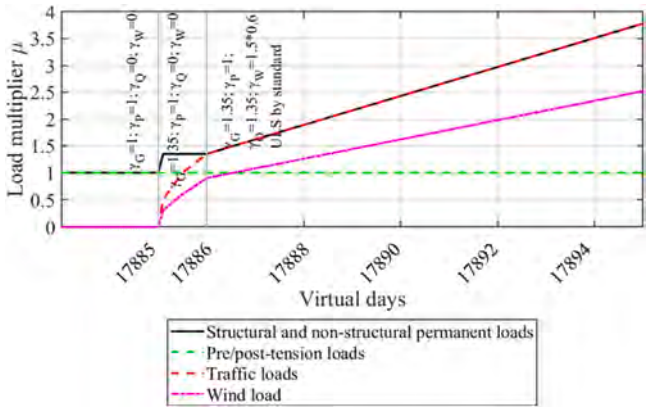

Fig. 11. Time-History of the load multiplier.

performed using the characteristic values of the material properties within the structural model; γ_{Rd} is the global safety factor of the model uncertainties (i.e., epistemic uncertainties) equal to 1.10.

If the design load multiplier of the structure obtained by the ECOV methodology is greater than the ULS design multiplier, calculated according to the design standard (Eq.(5)) and shown in Fig. 11, the structure can be considered safe at the ULS.

5. Results and discussion

This section deals with the results in terms of damage-dependent safety assessment of the deck and provides the definition of the damage thresholds in terms of specific static parameters for the type of structure under investigation.

5.1. Safety results with respect to the ULS

This subsection describes the results obtained from the safety assessment of the deck through the ECOV safety format considering both the undamaged and other nine damaged configurations.

For all the damage scenarios (i.e., Damage 1–9) in addition to the undamaged scenario, Table 12 reports the ultimate load multipliers achieved carrying out the 3D NLFEAs with the mean and characteristic material strengths, useful in the following to apply the ECOV methodology. The ultimate load multipliers are the same for both permanent and traffic loads, because the evolution of loads, after reaching the ULS combination according to the current standards, follows the same law, as can be seen in Fig. 11.

Regarding the undamaged scenario with the mean strength values, Fig. 13 shows stresses at the failure time, in concrete (Fig. 13(a)) and in pre-stressed strands and post-stressed cables (Fig. 13(b)). The maximum compressive stresses, leading to collapse, are reached in the concrete slab above external longitudinal beams (i.e., Beam 1 and Beam 2 of Fig. 4). For the beams denoted as "Beam 2 and Beam 3″ (Fig. 4), the pre-stressing and post-tensioning reinforcement reaches yield stress, whereas for the "Beam 1″ (Fig. 4) the values are close to the ultimate tensile strength. In all other models analysed, there are similar stress distributions at the collapse step with modifications in terms of failure mode, which can be steel-side or concrete-side as a function of the material properties, as explained in the following.

The results from the 20 3D NLFEAs (i.e., 9 damaged scenarios + 1 undamaged scenario considering both the mean and characteristic strength values) referred to the midspan section are shown in the following figures (i.e., Figs. 14–17). Fig. 14 shows the stresses at the bottom fiber of the edge beam (i.e., Beam 1). Fig. 15 shows the stresses at the top fiber of the same edge beam (i.e., maximum compressive stress). Fig. 16 shows the stresses in the post-tensioned cable for some damage scenarios since the post-tensioned cable in that section is completely

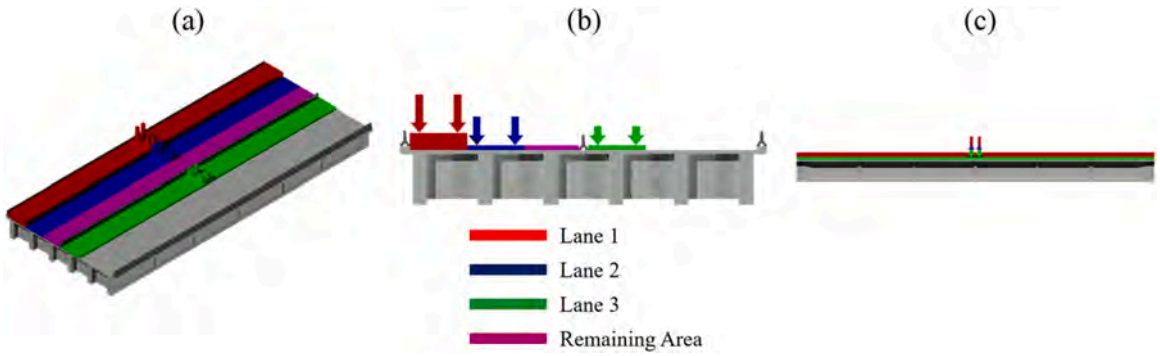

Fig. 12. Arrangement of traffic loads: (a) 3D view, (b) transverse view, (c) longitudinal view.

Table 12
Ultimate load multipliers.

Case	Permanent and traffic load multiplier with mean materials strength	Wind load multiplier with mean materials strength	Permanent and traffic load multiplier with characteristic materials strength	Wind load multiplier with characteristic materials strength
Undamaged	2.73	1.82	2.46	1.64
Damage 1	2.30	1.53	2.08	1.39
Damage 2	2.13	1.42	1.92	1.28
Damage 3	2.46	1.64	2.24	1.49
Damage 4	2.19	1.46	2.03	1.35
Damage 5	2.35	1.57	2.13	1.42
Damage 6	2.08	1.39	1.92	1.28
Damage 7	2.19	1.46	2.03	1.35
Damage 8	1.97	1.31	1.81	1.21
Damage 9 (ultimate condition)	1.76	1.17	1.59	1.06

removed for the models "Damage 2, 3, 4 and 9″. Fig. 17 shows the stresses in the pre-stressed strands. Collapse occurs with different resistance mechanisms in the different models with variable ductility. No brittle failure modes are observed due to the configurations of both loads and simulated damages, as described in the following:

- Undamaged scenario: concrete crush occurs in the slab above the edge beam;
- "Damage 1, 7 and 8″: the ultimate stress is reached in the pre-stressed strands and post-tensioned cable;
- "Damage 2, 4 and 9″: the ultimate stress is achieved in the pre-stressed strands;
- "Damage 3 and 5″: concrete crush occurs in the slab above the edge beam;
- "Damage 6″: the ultimate stress is reached in the post-tensioned cable.

In the scenarios with lower damage (i.e., Damage 3 and Damage 5), collapse occurs on the concrete-side reaching the ultimate compressive stress in the slab above the edge beam, whereas in presence of a more severe damage (i.e., Damage 1,2,4,6,7 and 9), collapse occurs on the steel-side reaching the ultimate strength of the pre-stressed strands and/or post-tensioned cable. In these last cases, the non-linear ductile capacities of the structural system are more involved.

Fig. 18 shows the structural behaviour for the different scenarios considered. It is possible to note that, for low load multipliers, the structural behaviour between undamaged and damaged decks is almost the same. The most marked differences appear when the load multiplier increases, therefore, when the material non-linearity field is reached. The undamaged deck shows great ductility, with an ultimate displacement of the edge beam bigger than 90 cm (i.e., 1/46 of the span). When the simulated damage level increases, this global ductility is lost, and the ultimate displacement is reduced to 50% less than the one in the sound condition.

Table 13 reports the design load multipliers following the application of the ECOV safety format calculated according to Eq. (7) on the basis of the results of Table 12. The variation with respect to the ultimate limit state condition imposed by the current standards is also listed in Table 13. These results show that the damaged structure still ensures good safety margins against the ULS. This safety result can be explained by the following factors:

- The deck has a high transverse structural redundancy, even if it is simply supported in longitudinal direction. Transverse redistribution allows for a load redistribution from the damaged lateral beam to the

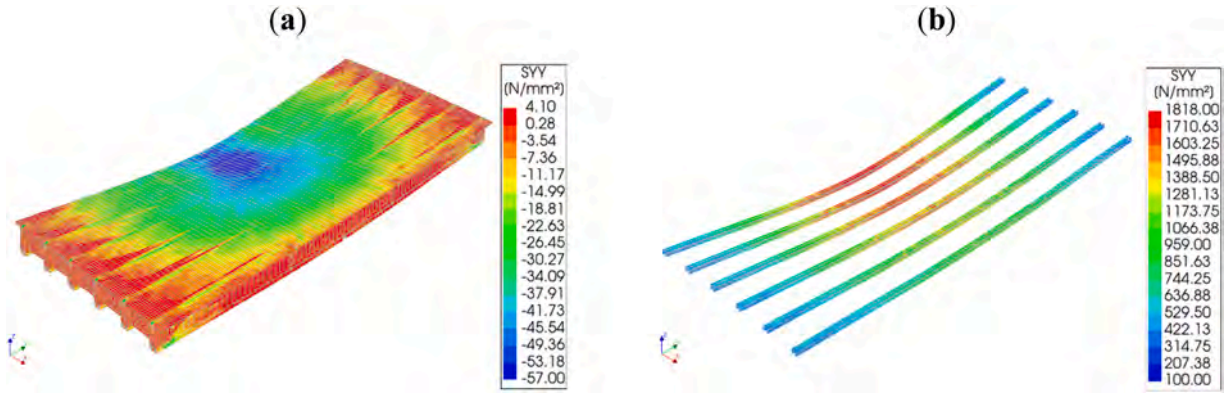

Fig. 13. Failure mode: (a) stresses in longitudinal directions in concrete, (b) stresses in pre-stressed strands.

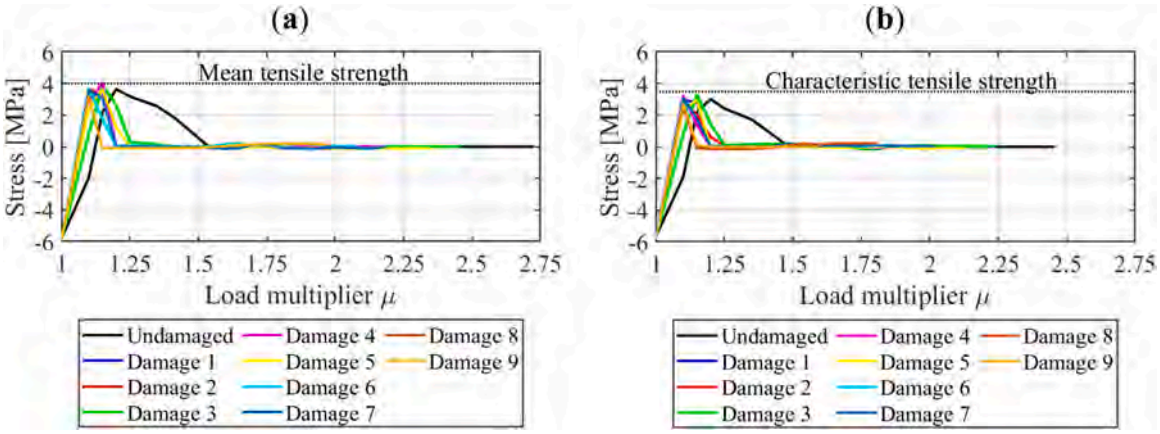

Fig. 14. Stresses in the bottom fiber of the edge beam: (a) model with the mean strengths of materials, (b) model with the characteristic strengths of materials.

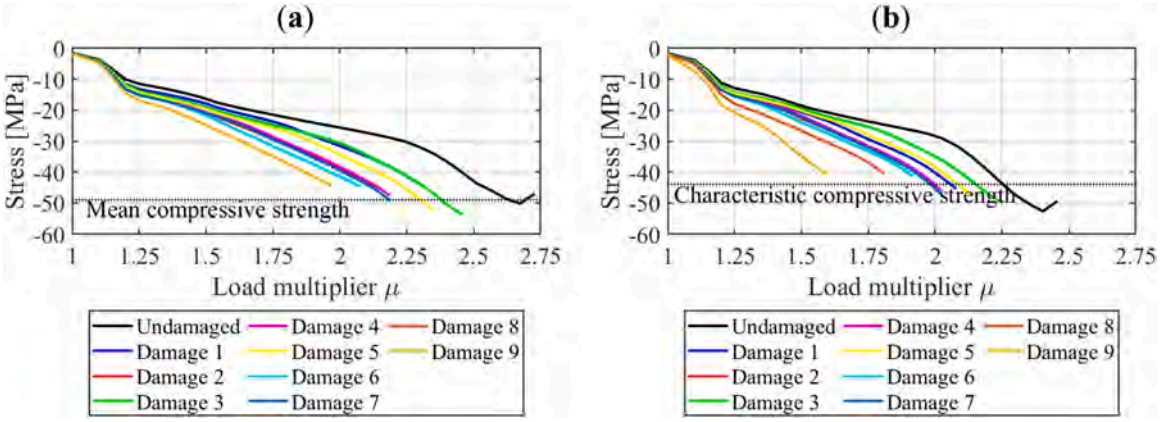

Fig. 15. Stresses at the top fiber of the edge beam: (a) model with the mean strengths of materials, (b) model with the characteristic strengths of materials.

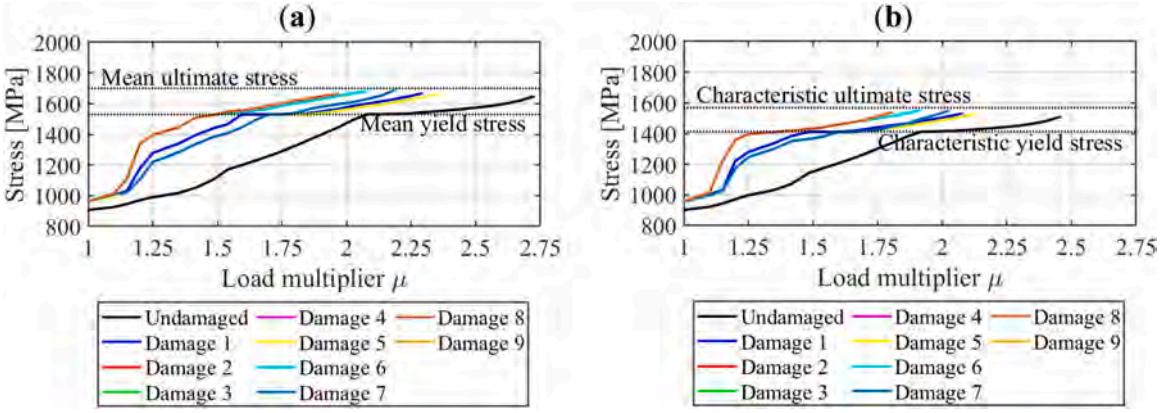

Fig. 16. Stresses in the post-tensioned cable: (a) model with the mean strengths of materials, (b) model with the characteristic strengths of materials.

sound central ones increasing the ULS performance of the deck. The three-dimensional model and the execution of a NLFE phased analysis made it possible to highlight this aspect, which was not considered in design and cannot be detected with the execution of standard linear analyses that provide results on safe side.

- As for both concrete and ordinary reinforcement steel, the mean and characteristic material strengths obtained from the test specimens taken during the in-situ testing campaign are higher than the original design strengths considered during the original design of the deck under investigation, as shown in Table 1.
- The stiffness of the 3D FE model is higher than that calculated using simplified models.
- The design actions calculated according to the standards in force at the time of the viaduct construction differ from those based on the standards currently in force. For example, the design bending moment in the middle section of the edge beam is approximately 15% higher than the bending moment in the same section calculated at the time of the viaduct's design.

The comparison in terms of safety factor is shown in Fig. 19. There are two limit scenarios: undamaged deck with an available safety factor

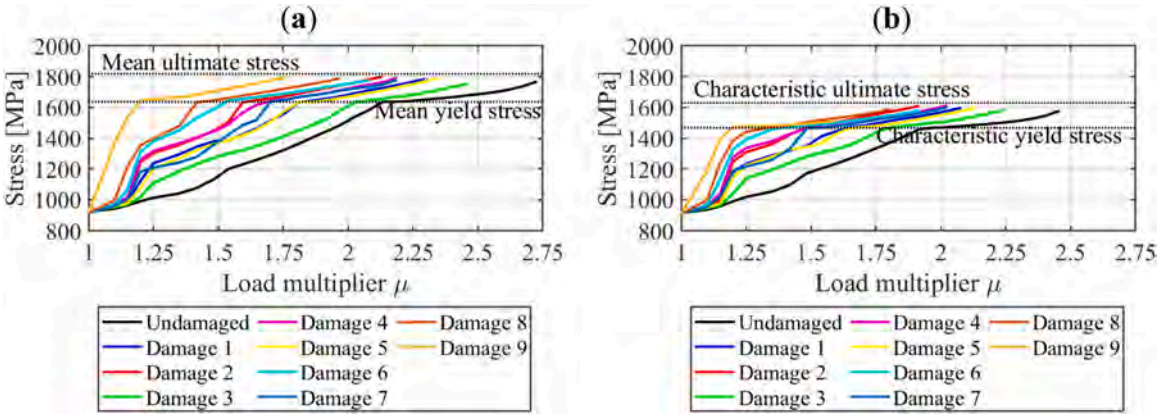

Fig. 17. Stresses in the pre-stressed strands: (a) model with the mean strengths of materials, (b) model with the characteristic strengths of materials.

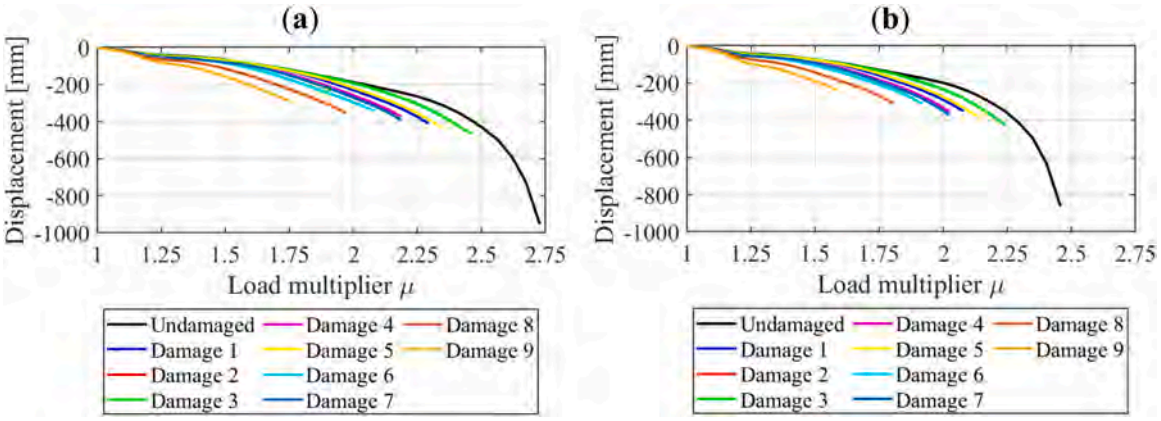

Fig. 18. Load-displacement curve for the longitudinal edge beam: (a) model with the mean strengths of materials, (b) model with the characteristic strengths of materials.

Table 13
Variation in load-bearing capacity compared to the ULS condition by standards.

Case	ECOV design permanent and traffic load multiplier	ECOV design wind load multiplier	Standards design permanent and traffic load multiplier	Standards design wind load multiplier	Safety margin with respect to code design
Undamaged	2.05	1.36	1.35	0.9	+ 51.9%
Damage 1	1.74	1.16	1.35	0.9	+ 28.9%
Damage 2	1.59	1.06	1.35	0.9	+ 17.8%
Damage 3	1.89	1.26	1.35	0.9	+ 40.0%
Damage 4	1.73	1.15	1.35	0.9	+ 28.1%
Damage 5	1.79	1.19	1.35	0.9	+ 32.6%
Damage 6	1.63	1.09	1.35	0.9	+ 20.7%
Damage 7	1.73	1.15	1.35	0.9	+ 28.1%
Damage 8	1.53	1.02	1.35	0.9	+ 13.3%
Damage 9 (ultimate condition)	1.35	0.9	1.35	0.9	0%

of 100% with respect to the ULS condition; "Damage 9″ has 0% available safety compared to the ULS condition. All the other damage scenarios (i.e., real and hypothesized ones) are in an intermediate condition. Damage 3 shows the smallest safety reduction (i.e., 77.1% available safety), whereas Damage 8 shows the highest effect on the safety of the deck (i.e., 25.7% available safety).

5.2. Damage thresholds

For each damage scenario, a 3D NLFEA is also carried out with the mean strengths of the materials and applying the loads of the load test shown in Fig. 9(i.e., lorries) used for the validation of the model. This analysis is performed to define damage thresholds in terms of measurable static parameters on the structure and is useful to detect the degradation phenomena and their possible evolution on the existing bridges similar to the system under investigation. These damage thresholds are represented in terms of rotations near the supports and displacements at the midspan. The limit rotation and displacement damage thresholds are evaluated on the model "Damage 9″. In fact, the application of LM1 leads this damaged model to the collapse of the structure at the ULS. Therefore, reaching those displacements/rotations under the loads of the load test (Fig. 9), in absence of traffic, should give a serious warning as the structure is not verified at the ULS with standard traffic loads.

Table 14 shows the rotations in the support zone (i.e., supports 1 and 2 that present the same rotations due to the symmetry of the load) and

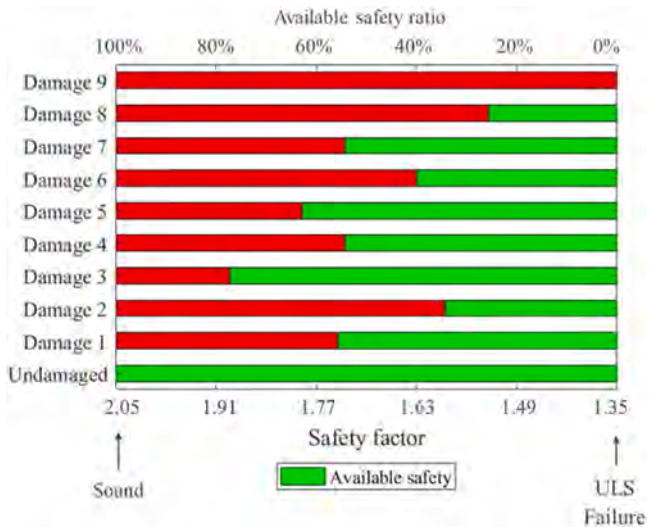

Fig. 19. Safety factor comparison for the damage scenarios.

Table 14
Rotation and displacement under test loads.

Case	Rotation at support [mrad]	Displacement at midspan [mm]
Undamaged	0.757	13.1
Damage 1	0.777	13.4
Damage 2	0.791	13.9
Damage 3	0.770	13.2
Damage 4	0.801	14.1
Damage 5	0.774	13.3
Damage 6	0.796	14.0
Damage 7	0.805	14.2
Damage 8	0.829	14.9
Damage 9	1.180	25.5

the displacements in the midspan of the deck for the different damage scenarios under the loads of the load test.

Fig. 20 shows a comparison of the different models in terms of displacements and rotations. The comparison between the different damage models in terms of displacements and rotations under the loads of the load test is shown respectively in Fig. 20(a) and in Fig. 20(b). The two limit conditions are: undamaged deck with an available displacement and rotation capacity of 100% and model "Damage 9″ with 0% available displacement and rotation capacity. All other damage scenarios represent an intermediate condition.

Depending on the importance of the structure, the displacement and rotation results from the load test with respect to specific simulated damage scenarios can represent thresholds to derive the damage on the structure. This procedure is useful for the evaluation of thresholds based on the damage level. In fact, during the in-situ test if the measured displacements/rotations are equal to those obtained with model "Damage 9″, the deck would have no margin of safety at the ULS. If the displacements/rotations during the in-situ test are the same as the one of the "Undamaged" model, no deterioration of the bridge stiffness is observed. The measurement of a displacement/rotation during an in-situ load test can be compared to the displacement/rotation of a NLFEA model with a damage simulation, and if the two results are similar, an estimation of the damage level can be deduced. All the simulated damages from 1 to 8 are examples of intermediate situations between "Undamaged" and "Damage 9" model that can be detected measuring the displacements/rotations through the set of lorries described in Fig. 9. It is important to underline that the presence of other damages in different positions of the structure (e.g., shear capacity reduction near a bearing of a beam) is not captured by these damage thresholds but may impact the bearing capacity of the structure.

6. Conclusions

This study proposes the evaluation of the structural safety of a bridge deck subjected to different damage scenarios by means of a global approach. For the safety assessment, 3D NLFEAs of the structure are performed and the ECOV safety format is implemented. Structural safety is assessed against the ULS condition provided by the current standards.

The damages simulated in this study decrease the bending resistance of the longitudinal edge beam of the deck. One of the damage scenarios (i.e., Damage 1) was really found on the structure. Seven (i.e., Damage 2 - Damage 8) were hypothesized by modifying the real one to consider some uncertainties highlighted during the qualitative inspections and assess the effects of different intensities and extensions of the observed damage. The last one (i.e., Damage 9) represents the ultimate limit damage for the safety of the structure at the ULS. They are simulated through the reduction of the ordinary and pre/post tension reinforcement area in the midspan of the beam.

The deck in its undamaged condition shows large safety margins against the ULS (i.e., +51.9% in terms of strength). The introduction of damage reduces the bearing capacity of the deck from 7.8% to 25.4% with respect to the undamaged deck condition, but in any case, there are safety margins with respect to the ULS from + 13.3% to + 40%, as reported in Table 13.

The results demonstrate that this type of deck can have a

Fig. 20. Comparison of the different damage scenarios under the test load: (a) displacements, (b) rotations.

considerable transverse load redistribution capacity. It should be emphasised, however, that this load redistribution capacity can only and exclusively be examined through detailed 3D NLFEAs, considering all the structural members working together, and depends on the geometry and reinforcement ratios of each single structure.

Any other, less refined, type of analysis would underestimate the load redistribution capacity and consequently drastically reduce the safety assessment of the structure with respect to the ULS. For these reasons, the use of refined analyses becomes essential for a more accurate assessment of the structural safety.

The structure studied in this paper has a large amount of pre/post tension reinforcement. This is probably the main reason for the structural safety level against the ULS even for extremely severe damage conditions on the side beam. It is of interest for the future to compare the following results with those of similar structures with damages like those simulated in this paper.

An extremely useful tool is also the definition of the damage thresholds. In fact, an assessment of the degradation of the structure can be obtained using in-situ load tests. The static parameters (displacements/rotations) under test loads (i.e., a set of lorries) and in absence of traffic loads can be measured and compared with the same static parameters obtained from the numerical models to obtain an estimation of the presence of a possible damage and its intensity. For the case study, different damage thresholds are proposed and can be used for similar bridges. Particularly, the limit damage is defined as the damage for which the structure presents no margin of safety against the ULS at the application of loads from LM1 (i.e., Damage 9). During the in-situ test if the measured displacements/rotations are equal to those obtained from the NLFE of the model “Damage 9″ with the test loads, the deck has no safety margin at the ULS.

Note that additional damages in different positions of the structure may have low or no effect on the static parameters of one beam but may impact the bearing capacity of the structure when loaded with different patterns. Furthermore, the measured displacements and rotations under the test loads do not evolve as a function of the damage linearly with the reduction of the safety coefficient. Therefore, a damage that generates a serious reduction in the safety coefficient may not be accompanied by an equally noticeable variation in the test displacements.

The procedure presented in this paper is useful to identify some damage levels in reinforcement arrangement and can be applicable to other bridge structures identifying specific damage thresholds depending on the type and importance of the structure. The results can be different from the ones achieved in this paper for differences in the geometry of the deck, the amount of prestressing reinforcement, construction phases and other specific characteristics of the bridge under exam.

Annex A

CRediT authorship contribution statement

Gabriele Bertagnoli: Conceptualization, Methodology, Writing - Original draft preparation, Supervision, Data curation, Writing - Reviewing and Editing, Investigation. **Mario Ferrara**: Conceptualization, Methodology, Software, Writing- Original draft preparation, Supervision, Data curation, Writing - Reviewing and Editing, Validation, Investigation. **Miceli Elena**: Conceptualization, Methodology, Writing - Original draft preparation, Supervision, Data curation, Writing- Reviewing and Editing, Validation, Investigation. **Castaldo Paolo**: Writing - Original draft preparation, Supervision, Writing - Reviewing and Editing. **Luca Giordano**: Conceptualization, Methodology, Supervision, Writing- Reviewing and Editing, Investigation.

Declaration of Competing Interest

No conflict of interest.

Data availability

Data will be made available on request.

Acknowledgements

This study was carried out within the Sustainable Mobility Center (CNMS) and received funding from the European Union Next Generation EU (Piano Nazionale di Ripresa e Resilienza (PNRR), Missione 4 Componente 2 Investimento 1.4 "Potenziamento strutture di ricerca e creazione di "campioni nazionali di R&S" su alcune Key Enabling Technologies") with grant agreement no. CN_00000023. This manuscript reflects only the authors’ views and opinions, neither the European Union nor the European Commission can be considered responsible for them.

This work is also part of the collaborative activity developed by the authors within the research project PRIN 2017 “*Life-long optimized structural assessment and proactive maintenance with pervasive sensing techniques*”.

This study was also carried out within the "*Data fusion based digital twins for structural safety assessment*" project – funded by European Union – Next Generation EU within the PRIN 2022 program (D.D. 104 - 02/02/2022 Ministero dell’Università e della Ricerca). This manuscript reflects only the authors’ views and opinions and the Ministry cannot be considered responsible for them.

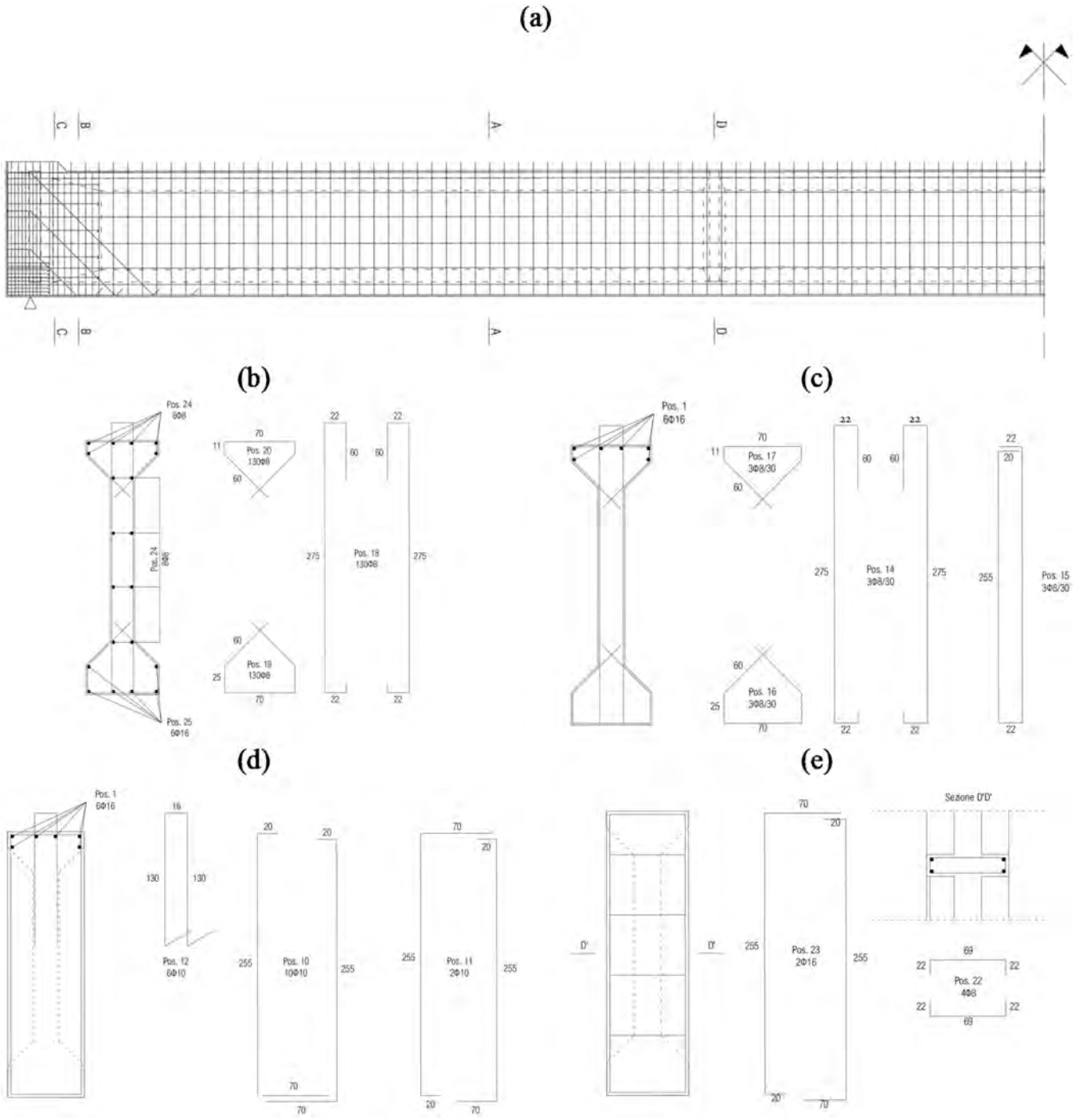

Fig. A1. Ordinary reinforcement arrangement in longitudinal beam: (a) longitudinal view, (b) cross-section A-A, (c) cross-section B-B, (d) cross-section C-C, (e) cross-section D-D. Measurements in centimetres with diameters in millimetres.

.

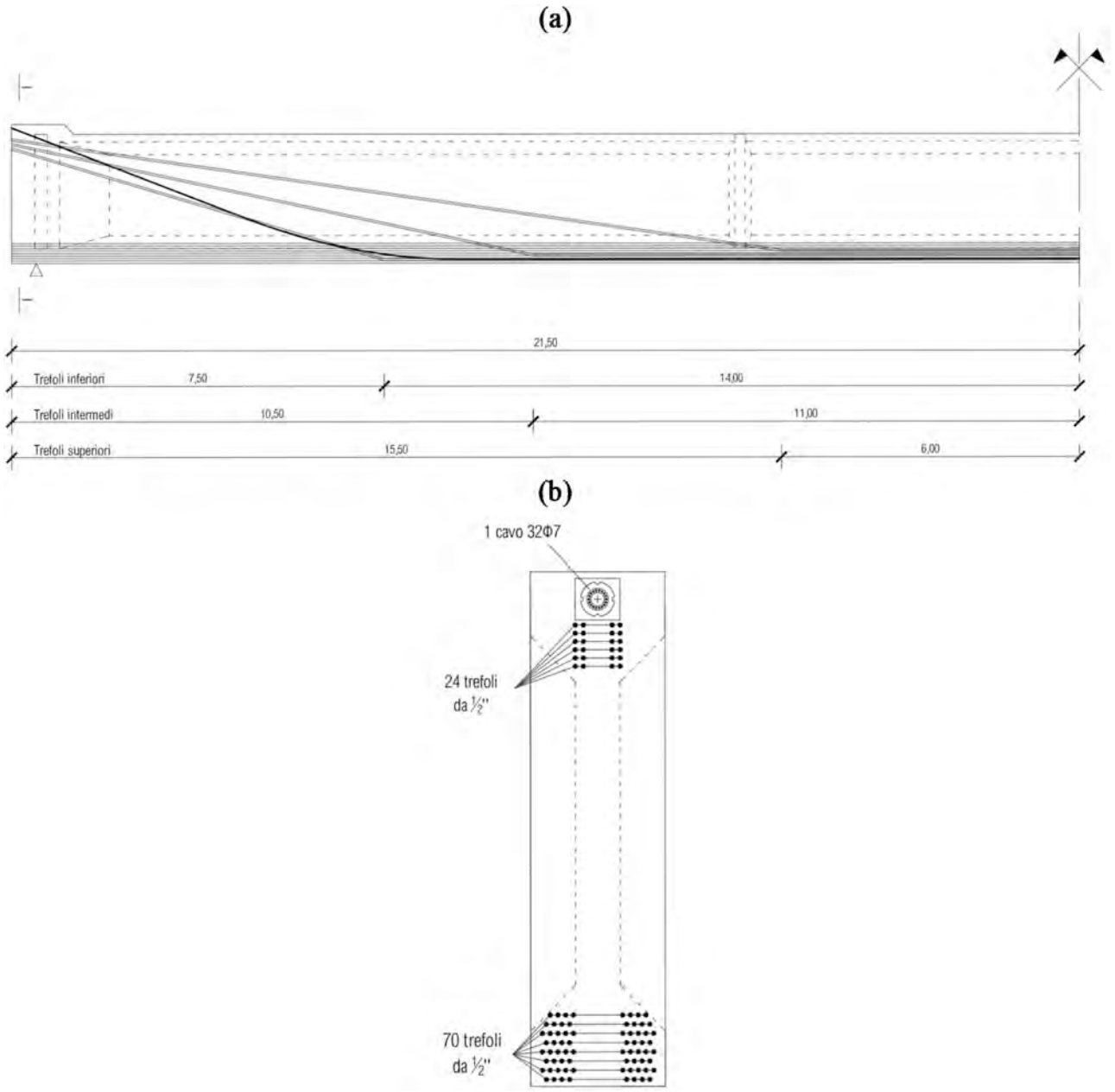

Fig. A2. Pre and Post-tension reinforcement arrangement in longitudinal beam: (a) longitudinal view, (b) cross-section I-I. Measurements in metres with diameters in millimetres or inches.

.

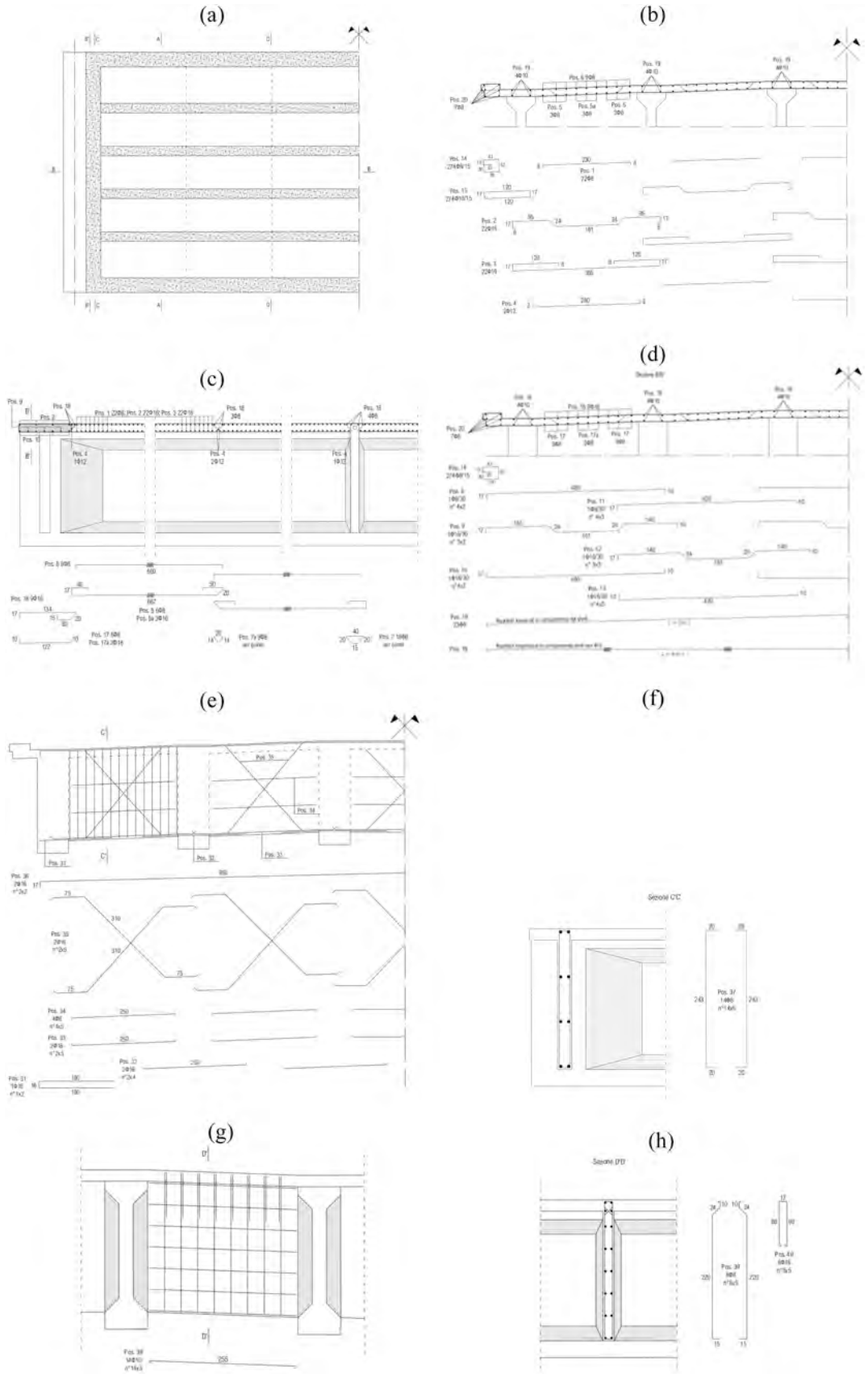

Fig. A3. Ordinary reinforcement arrangement in the slab and transverse beam: (a) planimetry, (b) section A-A, (c) section B-B. (d) section B′-B′, (e) section C-C, (f) section C′-C′, (g) section D-D, (h) section D′-D′. Measurements in centimetres with diameters in millimetres.

.

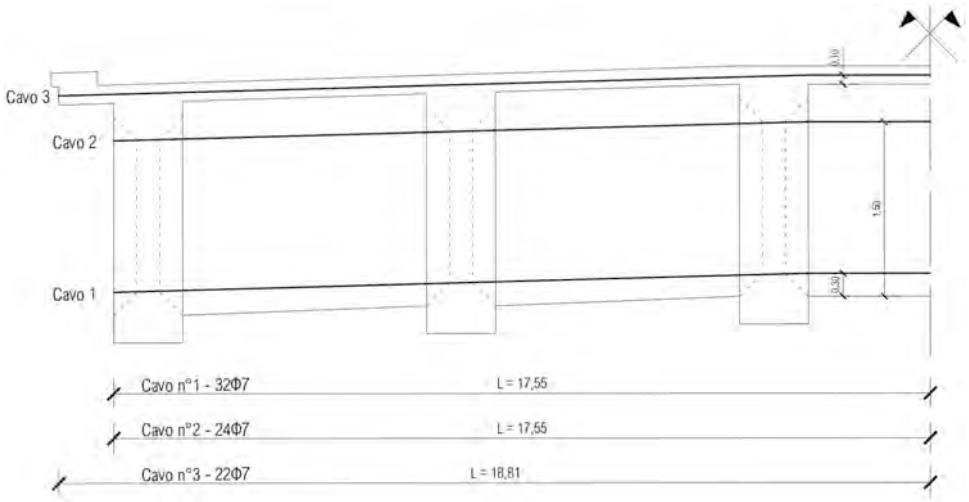

Fig. A4. Post-tension reinforcement arrangement in transverse beam and slab. Measurements in meters with diameters in millimetres.

.

References

[1] Neves LC, Frangopol DM. Condition, safety and cost profiles for deteriorating structures with emphasis on bridges. Reliab Eng Syst Saf 2005;89(2):185–98.
[2] Galano S, Losanno D, Miluccio G, Parisi F. Multidimensional nonlinear numerical simulation of post-tensioned concrete girders with different prestressing levels. Struct Concr 2023. https://doi.org/10.1002/suco.202300272.
[3] Repubblica Italiana - Ministero delle Infrastrutture e della Mobilità Sostenibili Consiglio Superiore dei Lavori Pubblici. Decreto numero 204 del 01–07-2022. Linee guida per la classificazione e gestione del rischio, la valutazione della Sicurezza ed il monitoraggio dei ponti esistenti.
[4] Cosenza E, Losanno D. Assessment of existing reinforced-concrete bridges under road-traffic loads according to the new Italian guidelines. Struct Concr 2021; Volume 22. https://doi.org/10.1002/suco.202100147.
[5] Miluccio G, Losanno D, Parisi F, Cosenza E. Fragility analysis of existing prestressed concrete bridges under traffic loads according to new Italian guidelines. Struct Concr 2023;24(1):1053–69.
[6] fib model code for concrete structures 2010. fib 2013. Lausanne.
[7] Muttoni A, Ruiz MF. Levels-of-approximation approach in codes of practice. Struct Eng Int J Assoc Bridge Eng 2012;22(2):190–4.
[8] Cervenka V. Reliability-based non-linear analysis according to *fib* Model Code. 2010. ISSN1464-4177 Struct Concr J *fib* 2011;14(2013):19–28.
[9] fib Bulletin N°45. Practitioner's guide to finite element modelling of reinforced concrete structures – state of the art report. Lausanne; 2008.
[10] Belletti B, Damoni C, Hendriks MAN. Development of guidelines for nonlinear finite element analyses of existing reinforced and prestressed beams. Eur J Environ Civ Eng 2011;15(9):1361–84.
[11] Most T. Assessment of structural simulation models by estimating uncertainties due to model selection and model simplification. Comput Struct 2011;89(17–18): 1664–72.
[12] Allaix DL, Carbone VI, Mancini G. Global safety format for non-linear analysis of reinforced concrete structures. Struct Concr 2013;14(1):29–42.
[13] Shlune H, Gylltoft K, Plos M. Safety format for non-linear analysis of concrete structures. Mag Concr Res 2012;64(7):563–74.
[14] Ftima MB, Massicotte B. Development of a reliability framework for the use of advanced nonlinear finite elements in the design of concrete structures. J Struct Eng 2012;138:1054–64.
[15] CEN EN 1992-2. Eurocode 2 – design of concrete structures, part 2: concrete bridges. Brussels: CEN,; 2005.
[16] Blomfors M, Engen M, Plos M. Evaluation of safety formats for non-linear finite element analyses of statically indeterminate concrete structures subjected to different load paths. Struct Concr 2016;17(1):44–51.
[17] Val D, Bljuger F, Yankelevsky D. Reliability evaluation in nonlinear analysis of reinforced concrete structures. Struct Saf 1997;19(2):203–17.
[18] Cervenka V. Reliability-based non-linear analysis according to *fib* Model Code 2010. Struct Concr 2013;14(1):19–28.
[19] Castaldo P, Gino D, Mancini G. Safety formats for non-linear finite element analysis of reinforced concrete structures: discussion, comparison and proposals. Eng Struct 2019;193:136–53.
[20] Červenka J, Červenka V, Sýkora M, Mlčoch J. Evaluation of safety formats for structural assessment based on nonlinear analysis. Comput Model Concr Struct 2018.
[21] Hasofer AM, Lind NC. Exact and invariant second moment code format. J Eng Div ASCE 1974;100(EM1):111–21.
[22] fib Bulletin No. 80. Partial factor methods for existing concrete structures; 2016. Available from: doi: 10.35789/fib.BULL.0080.
[23] Engen M, Hendriks MAN, Köhler J, Øverli JA, Åldtstedt E. A quantification of modelling uncertainty for non-linear finite element analysis of large concrete structures. Struct Saf 2017;64:1–8.
[24] Kadlec L, Červenka V. Model uncertainties of FEM nonlinear analyses of concrete structures. Solid State Phenom 2016;249:197–202.
[25] Gino D, Castaldo P, Giordano L, Mancini G. Model uncertainty in non-linear numerical analyses of slender reinforced concrete members. Struct Concr 2021.
[26] Engen M, Hendriks MAN, Monti G, Allaix DL. Treatment of modelling uncertainty of NLFEA in fib Model Code 2020. Structural Concrete, 22; 2021. p. 3202–12. https://doi.org/10.1002/suco.20210042032 12ENGENETAL.
[27] Castaldo P, Gino D, Bertagnoli G, Mancini G. Resistance model uncertainty in non-linear finite element analyses of cyclically loaded reinforced concrete systems. Eng Struct 2020;211:110496.
[28] Castaldo P, Gino D, Bertagnoli G, Mancini G. Partial safety factor for resistance model uncertainties in 2D non-linear finite element analysis of reinforced concrete structures. Eng Struct 2018;176.
[29] Gino G, Miceli E, Castaldo P, Recupero A, Mancini G. Strain-based method for assessment of global resistance safety factors for NLNAs of reinforced concrete structures. Eng Struct 2024;304:117625. https://doi.org/10.1016/j.engstruct.2024.117625.
[30] Miśkiewicz M, Bruski D, Chróścielewski J, Wilde K. Safety assessment of a concrete viaduct damaged by vehicle impact and an evaluation of the repair. Eng Fail Anal 2019;106:104147.
[31] Aktas M, Sumer Y. Nonlinear finite element analysis of damaged and strengthened reinforced concrete beams. ISSN 1392-3730 print/ISSN 1822-3605 online J Civ Eng Manag 2014;20(2):201–10. https://doi.org/10.3846/13923730.2013.801889.
[32] Belletti B, Vecchi F, Bandini C, Andrade C, Montero JS. Numerical evaluation of the corrosion effects in prestressed concrete beams without shear reinforcement. Struct Concr 2020;21:1794–809.
[33] Bertagnoli G, Ferrara M, Giordano L, Malavisi M. Preliminary investigation on steel jacketing retrofitting of concrete bridges half-joints. Appl Sci 2023;13:8181. https://doi.org/10.3390/app13148181.
[34] Belletti B., Damoni C., Hendriks M. Non-linear finite element analyses of existing reinforced concrete bridge beams. In: proceedings of the IABSE conference: assessment, upgrading and refurbishment of infrastructures, Rotterdam, The Netherlands, 6–8 May 2013, published in Assessment, Upgrading and Refurbishment of Infrastructures, pp. 520–21.
[35] EN 1992: Eurocode 2: design of concrete structures - Part 1–1: General rules and rules for buildings, UNI.
[36] Holicky M, Materna A, Sedlacek G, Arteaga A, Sanpaolesi L, Vrouwenvelder T, et al. Implementation of eurocodes: handbook 2: Reliability backgrounds, Leonardo Da Vinci pilot project CZ/02/B/F/PP-134007.
[37] EN 1990: Eurocode 0: basis of structural design, European Standard; 2002.
[38] Theory manual of DIANA FEA, Release 10.2, DIANA FEA BV.
[39] Element library of DIANA FEA, release 10.2, DIANA FEA BV.
[40] Rashid Y. Analysis of prestressed concrete pressure vessels. Nucl Eng Des 1968;7: 334–44.
[41] Cervera M, Chiumenti M. Smeared crack approach: back to the original track. Int J Numer Anal Meth Geomech 2006;30:1173–99.

[42] Vecchio FJ, Collins MP. The modified compression field theory for reinforced concrete elements subjected to shear. Acids J 1986;83(22):219–31.
[43] Selby RG, Vecchio FJ. Three-dimensional constitutive relations for reinforced concrete. Tech. Rep. 93-02. Toronto, Canada: Univ. Toronto, Dept. Civil Eng.; 1993.
[44] Miceli E, Castaldo P. Robustness improvements for 2D reinforced concrete moment resisting frames: parametric study by means of NLFE analyses. 2024 Struct Concr 2023;25:9–31. https://doi.org/10.1002/suco.202300443.
[45] Material library of DIANA FEA, release 10.2, DIANA FEA BV.
[46] Vecchio FJ, Collins MP. Compression response of cracked reinforced concrete. J Str Eng, ASCE 1993;119(12):3590–610.
[47] Selby RG, Vecchio FJ. A constitutive model for analysis of reinforced concrete solids. Can J Civ Eng 1997;24:460–70.
[48] Mises R v. "Mechanik der festen Körper im plastisch- deformablen Zustand." Nachrichten von der Gesellschaft der Wissenschaften zu Göttingen. Math-Phys Kl 1913;1913:582–92.
[49] Ford H, Alexander JM. Advanced mechanics of materials. London: Longmans; 1963.
[50] NTC 2018. Norme Tecniche per le Costruzioni. Technical Standards for Construction. Off J Ital Repub 2018.
[51] EN 1991–2, Eurocode 1–part 2. Traffic actions on bridges.
[52] Bertagnoli G., Ciccone E., Ferrara M. Structural Health Monitoring of a prestressed concrete bridge deck. In: Proceedings of the Italian concrete conference 2022 Ed. By Aiello M. A., Bilotta A., Springer Nature, in print.
[53] Du YG, Clark LA, Chan AHC. Effect of corrosion on ductility of reinforcing bars. Mag Concr Res 2005;57(7):407–19.
[54] Apostolopoulos CA, Papadakis VG. Consequences of steel corrosion on the ductility properties of reinforcement bar. Constr Build Mater 2008;22(12):2316–24.
[55] R. Hingorani, J. Fullea, J. Sanchez, C. Andrade. Loss of ductility and strength of reinforcing steel due to pitting corrosion. In: Proceedings of the eighth international conference on fracture mechanics of concrete and concrete structures.
[56] Franceschini L, Belletti B, Tondolo F, Montero JS. A simplified stress–strain relationship for the mechanical behavior of corroded prestressing strands: The SCPS-model. Struct Concr 2022;24(1):189–210.